Heliyon 10 (2024) e32523

Contents lists available at ScienceDirect

Heliyon

journal homepage: www.cell.com/heliyon

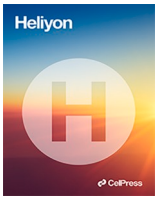

Research article

Efficacy of *Rhamnus utilis* Decne. Aqueous extract in mice with acute alcoholic liver injury and metabolomic study

Xianglong Meng [a,b], Kele Ren [a,b], Xiaoqin Liu [a,b,c], Chenzi Lyu [d], Hyo Won Jung [d,**], Yilong Zhang [e], Shuosheng Zhang [a,b,*]

[a] *College of Chinese Materia Medica and Food Engineering, Shanxi University of Chinese Medicine, Jinzhong, 030619, Shanxi, China*
[b] *Shanxi Key Laboratory of Traditional Herbal Medicines Processing, Jinzhong, 030619, Shanxi, China*
[c] *College of Pharmacy, Shandong Modern University, Jinan, 250104, China*
[d] *Department of Herbology, College of Korean Medicine, Dongguk University, Gyeongju, 38066, South Korea*
[e] *Shanxi Pengyakang Biotechnology Co., Ltd, Lyuliang, 033000, Shanxi, China*

ARTICLE INFO

Keywords:
Alcoholic liver injury
MAPKs/NF-κB/COX-2-iNOS
Anti-inflammation

ABSTRACT

Rhamnus utilis Decne. (Family Rhamnaceae Juss.) leaf is commonly prepared as a anti-inflammatory herbal medicine and used for tea production. To investigate the mechanism of *Rhamnus utilis* Decne. aqueous extract (RDAE) against acute alcoholic liver disease (ALD) in mice. The ALD mouse (Male ICR) model was induced via intragastric administration of 52 % alcohol. Mice in each group were treated by gavage once daily with the RDAE (1.12, 2.25, 4.500 g/kg). The expression of proteins involved in the MAPKs/NF-κB/COX-2-iNOS pathway was measured by western blotting. Non-targeted metabolomics was used to determine metabolic profiles and critical pathways, while targeted metabolomics validated key amino acid metabolites. After administration of RDAE, the body mass of mice was significantly increased. The liver index was significantly decreased. Meanwhile, the serum levels of AST, ALT, TG, TC, MDA, TNF-α, IL-1β and IL-6 were significantly decreased ($P < 0.05$, $P < 0.01$), but GSH level was inversely increased ($P < 0.05$). Metabolomic analysis revealed nine major pathways involved in the therapeutic effect of RDAE, including fructose and mannose metabolism. The levels of 7 amino acids including leucine, proline and alanine/sarcosine were significantly upregulated. Additionally, protein levels of p–NF–κB (p65)/NF-κB (p65), *p*-$ERK_{1/2}$/$ERK_{1/2}$, *p*-JNK/JNK, p-p38/p38, COX-2 and iNOS were significantly decreased ($P < 0.01$, $P < 0.05$). RDAE is used to treat acute ALD by improving lipid metabolism, inhibiting the expression of pro-inflammatory cytokines and regulating MAPKs/NF-κB/COX-2-iNOS signalling pathway. These findings provide valuable insights for acute ALD therapy based on traditional Chinese medicine (TCM).

1. Introduction

Alcoholic liver disease (ALD) is a prevalent global liver diseases characterized by a long and recurrent disease course, as well as refractoriness. It poses a high risk of progression to fatty liver cirrhosis and even liver cancer [1]. The incidence of ALD is positively associated with the amount of alcohol consumed [2]. According to the *Global Status Report on Alcohol and Health 2018* released by the

* Corresponding author. College of Shanxi University of Chinese Medicine, Jinzhong, 030619, China.
** Corresponding author.
E-mail addresses: tenzing2@hanmail.net (H.W. Jung), zhangshuosheng@aliyun.com (S. Zhang).

https://doi.org/10.1016/j.heliyon.2024.e32523
Received 11 December 2023; Received in revised form 4 June 2024; Accepted 5 June 2024
Available online 6 June 2024

World Health Organization (WHO), excessive alcohol consumption leads to approximately 3 million people deaths worldwide [3]. ALD encompasses both acute and chronic forms, with acute ALD referring to severe liver injury resulting from a high dose of alcohol consumed within a short period. This leads to an increased production of lipid metabolites through ethanol metabolism *in vivo*, triggering cascade reactions that contribute to the development of liver injury [4]. In the initial stages of acute ALD, oxidative stress plays a crucial role by causing damage to intracellular macromolecules and organelles, inducing lipid peroxidation in biomembranes [5,6], inflammatory responses [7], and apoptosis. The MAPK signaling pathway is intricately associated with inflammation and oxidative stress. NF-κB (p65) can elicit the expression of multiple genes by activating stimulating factors such as viruses, tumor necrosis factor, B-cell activating factor, lymphotoxin, etc., thereby generating a diverse array of cytokines involved in inflammation [8,9]. In the process of liver injury, there is a significant increase in the phosphorylation level of p38 MAPK, leading to the induction of NF-κB (p65) phosphorylation and subsequent release of a plethora of inflammatory factors by liver cells. This cascade results in oxidative and inflammatory damage to the liver. The expression of COX-2 exhibits a positive correlation with hepatocyte injury severity, and inhibition of COX-2 expression can effectively mitigate hepatic inflammatory infiltration. Furthermore, iNOS, an important downstream signaling molecule regulated by NF-κB activation, stimulates nitric oxide (NO) production which can induce liver damage through oxidative stress or neutrophil adhesion activation [10]. Both iNOS and COX-2 expressions are induced via NF-κB signaling. These reactions can significantly impact the metabolism of sugars, lipids, and amino acids, thereby exacerbating liver injury through accelerated metabolite accumulation. Current clinical agents for ALD treatment exhibit drawbacks such as drug resistance and potential drug-induced diseases. Hence, there is an urgent need for highly efficient natural herbal medicines with minimal toxic side effects to effectively address ALD.

Rhamnus utilis Decne. (Rhamnaceae) fruits and leaves are commonly utilized in the preparation of anti-inflammatory herbal medicines and for tea production. This plant is widely distributed in the northern and northwestern provinces of China, with abundant resources. Both traditional Chinese and modern medicine recognize the potential benefits of *Rhamnus utilis* Decne., including pain relief and promotion of digestion [11]. Therefore, it is commonly employed to facilitate digestion, counteract the effects of alcohol, safeguard hepatic function, attenuate the activity of associated enzymes, and confer protection against viral invasion [12]. Modern investigations have unveiled that *Rhamnus utilis* Decne. leaves harbor a profusion of chemical constituents including flavones, polyphenols, polysaccharides, glycosides, phenols, organic acids, and tannin [13], which underlie their pharmacological attributes with particular emphasis on anti-inflammatory and antioxidant properties [14]. In addition, *Rhamnus utilis* Decne. leaves exhibit hepatoprotective effects against CCL4-induced liver injury [15]. A murine study has demonstrated that *Rhamnus utilis* Decne. leaves can also ameliorate alcohol-induced liver injury in mice [16]. However, there remains a paucity of Chinese studies elucidating the mechanistic basis for the therapeutic efficacy of *Rhamnus utilis* Decne. leaves in treating liver injury.

The present study employed intragastric alcohol administration to model acute ALD in mice. Subsequently, *Rhamnus utilis* Decne. aqueous extract (RDAE) was administered, followed by an analysis of serum biochemical indices and inflammatory factors and observation of histopathological changes in liver tissues. Non-targeted metabolomic analysis was utilized to profile global metabolism, while targeted metabolomic analysis was employed to validate vital metabolic pathways involved in amino acid metabolism. Furthermore, the impact of inflammation on the liver was assessed through the expression of proteins associated with the MAPKs/NF-κB/COX-2-iNOS signaling pathway, aiming to elucidate the underlying mechanism behind the therapeutic effect of RDAE against acute ALD. The findings from this study are anticipated to provide experimental and theoretical evidence for future development of functional foods derived from *Rhamnus utilis* Decne. leaves.

2. Materials

2.1. Materials and reagents

Rhamnus utilis Decne. leaves were obtained from Lyuliang City, Shanxi Province, China, and were identified as dry leaves of *Rhamnus utilis* Decne. of the Rhamnaceae Juss. Family by Professor Shuosheng Zhang of the Shanxi University of Chinese Medicine. The voucher specimen is stored in the Herbarium of the Herbarium of Shanxi College of Traditional Chinese Medicine (SXTCM), Taiyuan, China (No. SXTCM-Zhang-2021012).

Silymarin (SIL; No. C10742879, Macklin, Shanghai, China), Red Star Erguotou 52° (RedStarWine, Beijing, China), alanine aminotransferase (ALT), aspartate aminotransferase (AST), triglycerides (TG), total cholesterol (TC), malondialdehyde (MDA), glutathione (GSH) (No. 20210719, No. 20210630, No. 20201015, No. 20210716, No. 20201021, No. 20210717, Nanjing Jiancheng Bioengineering Institute, Nanjing, China), tumor necrosis factor α (TNF-α), interleukin-1β (IL-1β), IL-6 (No. 202112, No. 202201, No. 202201, Shanghai Enzyme-linked Biotechnology Co., Ltd., Shanghai, China), HRP-conjugated goat anti-rabbit IgG (No. BA1055, Boster, Wuhan, China); β-actin, NF-κB (p65), p–NF–κB (p65), p38, p-p38, *p*-$ERK_{1/2}$, $ERK_{1/2}$, *p*-JNK, JNK, COX-2, and iNOS (No. AP0060, No. A2547, No. AP0475, No. AP0545, No. AP0073, No. AP0424, No. AP0715, No. A3254, No. A0215, Boster, Wuhan, China), acetonitrile (No. 1499230-935, Merck, St. Louis, MO, USA), ammonium acetate (No. 73594, Sigma-Aldrich, St. Louis, MO, USA), formic acid (No. 06450, Fluka, Seltzer, Germany), and methanol (No. 144282, Merck, St. Louis, MO, USA).

2.2. Instruments

RE-2000B rotatory evaporator (Shanghai Yarong Biochemistry Instrument Factory, Shanghai, China), TGL16 M high-speed refrigerated centrifuge (CenLee, Hunan, China); GeneGnome imaging system (GeneGnome XRQ, Gene, USA), Q Exactive series mass spectrometer (Thermo Fisher Scientific, MA, USA), Agilent 1290 Infinity LC ultra-high-pressure liquid chromatograph (Agilent

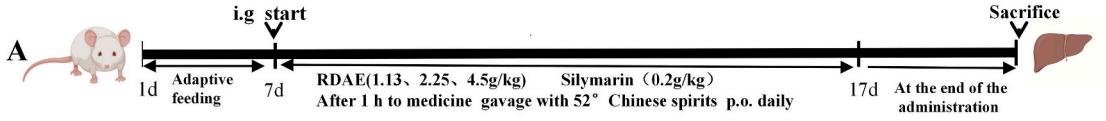

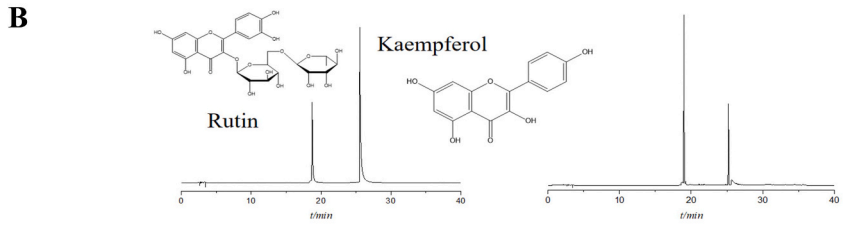

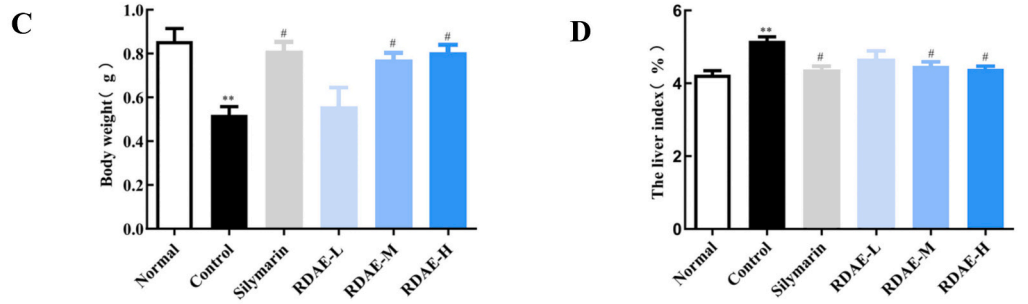

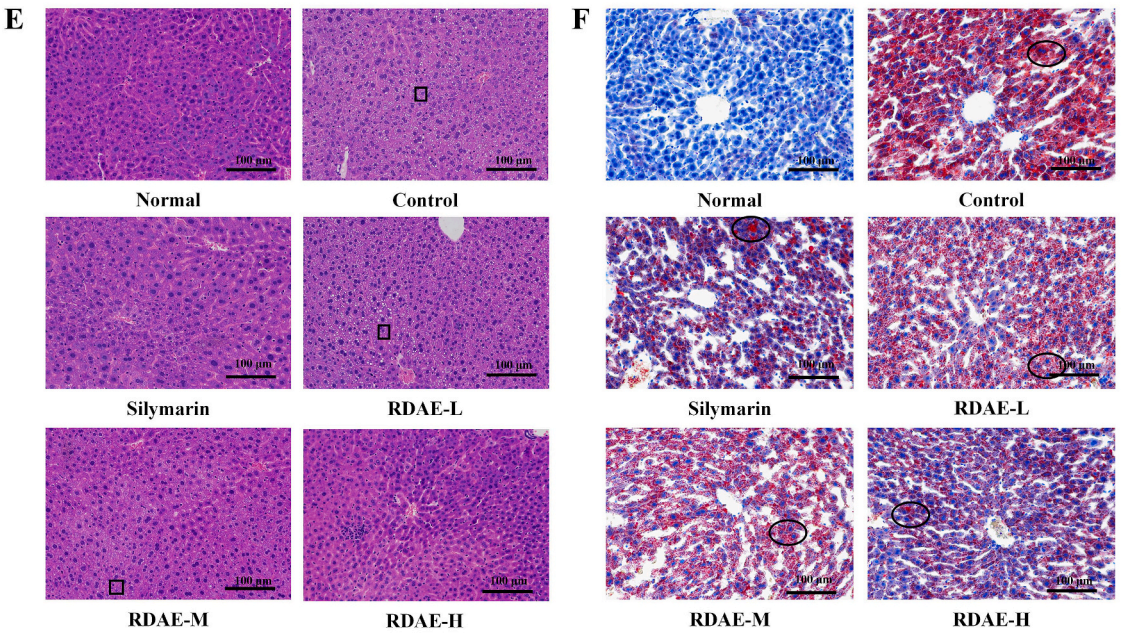

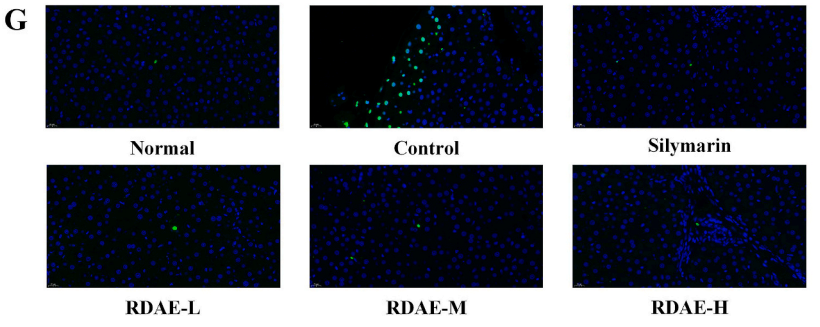

(caption on next page)

Fig. 1. Effects of *Rhamnus utilis* Decne aqueous extract in mice with acute alcoholic liver injury. (A) Establishment of acute alcoholic liver injury model in mice, (B) HPLC, (C) Body Weight ($\bar{x} \pm s$, n = 10), (D) The liver index ($\bar{x} \pm s$, n = 10), (E) HE staining, 200 × , (F) Oil-Red-O staining, 200 × . Normal: blank, control: model, silymarin: positive, RDAE-L: low-dose RADE, RDAE-M: medium-dose RADE, RDAE-H: high-dose RADE, pane: Hepatocytes exhibited vacuolationred, circle: Lipid droplets. $^{*}P < 0.05$, $^{**}P < 0.01$ *vs.* Normal group. $^{\#}P < 0.05$, $^{\#\#}P < 0.01$ *vs.* Control group. (For interpretation of the references to color in this figure legend, the reader is referred to the Web version of this article.)

Technologies Co. Ltd., Palo Alto, CA, USA), low-temperature high-speed centrifuge (Eppendorf5430R, Hamburg, Germany).

2.3. Experimental animals

Male ICR mice (SPF-grade, 20 ± 5 g) were provided by Si Pei Fu (Beijing, China) (License No. SCXK-Jing-2019-0010; certificate No. 110324210102969025). All animal procedures followed the Animal Research Reporting In *Vivo* Experiments Guidelines (ARRIVE) with the approval of the Ethics Committee of the Shanxi University of Chinese Medicine (No. 2021DW261). During the experiment, all mice were housed in a clean-grade animal room with ad libitum access to food and water at a temperature of 20–26 °C and humidity of 40%–70 %.

3. Methods

3.1. Quality representation of RDAE

The fresh leaves were subjected to oven drying, followed by crushing and sieving through a 70 mesh sieve. Subsequently, the resulting powder (10 g) was refluxed in 300 mL of distilled water at 60 °C for two cycles of 2 h each. After filtration, the solution was concentrated to a concentration of 1 g/mL and refrigerated for subsequent analysis.

The determination of total flavone content in RDAE was performed using high-performance liquid chromatography (HPLC) [17].

3.2. Grouping and drug administration

ICR mice (n = 60) were allowed to acclimate for seven days and equally divided into the Blank, Control, SIL (0.2 g/kg), RDAE-L (low-dose RDAE, 1.125 g/kg), RDAE-M (medium-dose RDAE, 2.250 g/kg), and RDAE-H (high-dose RDAE, 4.500 g/kg) groups (n = 10 for each group). Acute ALD was induced in mice based on the literature [18]. Mice in each group received daily oral administration of the corresponding agent via gavage. Additionally, apart from the Normal group, mice from other groups were subjected to intragastric administration of 12 mL/kg liquor (alcohol concentration: 52 %) 1 h after gavage for ten consecutive days (Fig. 1A).

After the previous administration, mice were anesthetized using ether. Blood samples were collected from the abdominal aorta and incubated at room temperature for 30 min, followed by centrifugation at 3000 rpm at 4 °C for 15 min. The resulting serum was stored in a freezer at −80 °C. The liver was isolated, with the left lobe preserved in tissue fixation solution at room temperature while the remaining portion was stored in a freezer at −80 °C.

Body mass change was recorded as mean daily weight gain (g) = mean overall weight gain (g)/growth days (d). The visceral (liver) index (%) was calculated as liver weight (g)/body weight (g) × 100 %.

3.3. Hematoxylin & eosin (H&E) staining

The liver was fixed, dehydrated, rendered transparent, and embedded in paraffin. H&E staining was performed, followed by digital slide image scanning and analysis using a computerized system. Hepatic tissue morphology was observed.

3.4. Oil-Red-O staining

The same liver section from each group was frozen, sectioned, and stained with an Oil-Red-O solution for 10 min. Subsequently, the sections were rinsed with 60 % isopropanol until clear interstitial staining appeared before being washed with distilled water. Finally, the sections were sealed with glycerol-gelatin and examined under an inverted microscope.

3.5. Terminal deoxynucleotidyl transferase dUTP nick end labeling (TUNEL)

Liver samples from each mouse were preserved in cassettes in Tissue-Teck (Sakura Finetek U.S.A, Torrance, CA) at −80 °C. TUNEL tests were performed by standard procedures following the manufacturer's protocol (Roche, Rotkreuz, Switzerland) [19].

3.6. Biochemical analysis

The serum levels of ALT, AST, TG, TC, MDA, and GSH were determined following the manufacturer's instructions.

3.7. Examination of inflammatory factors

The serum levels of TNF-α, IL-1β, and IL-6 were determined using corresponding enzyme-linked immunosorbent assay (ELISA) Kits.

3.8. Non-targeted metabolomics

3.8.1. Sample processing

Frozen liver samples were thawed at 4 °C. Then, 100 mg of the sample was treated with a pre-cooled methanol/acetonitrile/water solution (2:2:1, v/v). The mixture was rotated, sonicated at a low temperature for 30 min, kept at −20 °C for 10 min, and centrifuged at 12,000 rpm at 4 °C for 20 min. The supernatant was collected and evaporated to dryness. Mass spectrometry (MS) was performed by adding 100 μL of acetonitrile aqueous solution (acetonitrile: water = 1:1, v/v). The mixture was then rotated and centrifuged at 14,000 rpm and 4 °C for 15 min, and the supernatant was collected for further analysis.

3.8.2. Mass spectrometric and chromatographic operating conditions

Chromatographic separation was performed using the Agilent 1290 Infinity LC ultrahigh-performance liquid chromatography (UHPLC) HILIC chromatography column with the following parameters: column temperature, 25 °C; sample injection volume, 2 μL; gradient elution conditions (mobile phase A: water + 25 mM ammonium acetate + 25 mM aqueous ammonia; mobile phase B: acetonitrile): 95 % B from 0 to 0.5 min, 95 % B to 65 % B from 0.5 to 7 min, 65 % B to 40 % B from 7 to 8 min, 40 % B from 8 to 9 min, 40 % B to 95 % B from 9 to 9.1 min, and 95 % B from 9.1 to 12 min.

Metabolites were determined using a Q Exactive Series mass spectrometer with the following parameters: positive and negative ion source voltage = ±5500 V, ion source temperature = 600 °C, de-clustered voltage = ±60 V, collision energy = (35 ± 15) eV, auxiliary gas 1 (Gas 1) = 60 psi, auxiliary gas 2 (Gas 2) = 60 psi, curtain gas (CUR) = 30 psi, range of primary mass-to-charge ratios (m/z) = 60–1000 Da, range of secondary m/z = 25–1000 Da, primary MS scan accumulation time = 0.20 s/spectra, secondary MS scan accumulation time = 0.05 s/spectra, information-dependent acquisition (IDA) settings: dynamic exclusion of isotopes within 4 Da, and collection of 10 fragment ions per scan [20,21].

3.8.3. Data processing

Raw metabolomic data were obtained and converted into. mzXML format using ProteoWizard and processed using the XCMS platform to align peaks, correct retention time, and extract peak area. The data extracted from the XCMS platform were used for metabolite structural identification, data preprocessing, quality assessment, and statistical analysis.

3.9. Quantitative analysis of amino acids and derivatives in liver

3.9.1. Extraction of metabolites

A frozen liver sample (60 mg) was mixed with 50 μL MP-water homogenate, rotated for 60 s, and 400 μL methanol-acetonitrile aqueous solution (1:1, v/v) was added, followed by 50 μL (50 μm mixture of 16 internal standard isotopes). The mixture was rotated for 60 s, sonicated twice at low temperature for 30 min, kept at −20 °C for 1 h, and then centrifuged at 14,000 rpm at 4 °C for 20 min. The supernatant was collected, freeze-dried, and stored at −80 °C.

3.9.2. Mass spectrometric and chromatographic operating conditions

Chromatographic separation was achieved using an Agilent 1290 Infinity LC UHPLC with the following parameters: column temperature = 40 °C, sample injection volume = 1 μL, gradient elution (mobile phase A: 25 mM ammonium formate + 0.08 % FA aqueous solution; mobile phase B:0.1 % FA acetonitrile): 90 % B to 70 % B from 0 to 12 min, 70 % B to 50 % B from 12 to 18 min, 50 % B to 40 % B from 18 to 25 min, 40 % B to 90 % B from 30 to 30.1 min, and 90 % B from 30.1 to 37 min.

MS analysis was performed in positive ion mode (PIM) using a 5500 QTRAP mass spectrometer (AB SCIEX) with the following ESI source conditions: source temperature = 500 °C, gas 1 = 40 psi, gas 2 = 40 psi, CUR = 30 psi, ion Sapary Voltage Floating (ISVF) = 5500 V.

3.9.3. Data processing

Metabolic pathway enrichment analysis was performed using the Metabo Analyst 5.0 database (https://www.metaboanalyst.ca/home.xhtml). The area and retention time of the chromatographic peaks were determined using MultiQuant (Oxford Instruments, Shanghai, China). Retention time was corrected based on standard amino acids and derivatives for metabolite identification.

3.10. Western blotting

Protein levels of p-ERK$_{1/2}$/ERK$_{1/2}$, p-JNK/JNK, p-p38/p38, p–NF–κB (p65)/NF-κB (p65), COX-2 and iNOS in liver tissues were measured as previously described [19,20].

3.11. Statistical analysis

Data from efficacy experiments, shown as $\bar{x} \pm s$ and conforming to the homogeneity of variance, were processed using GraphPad

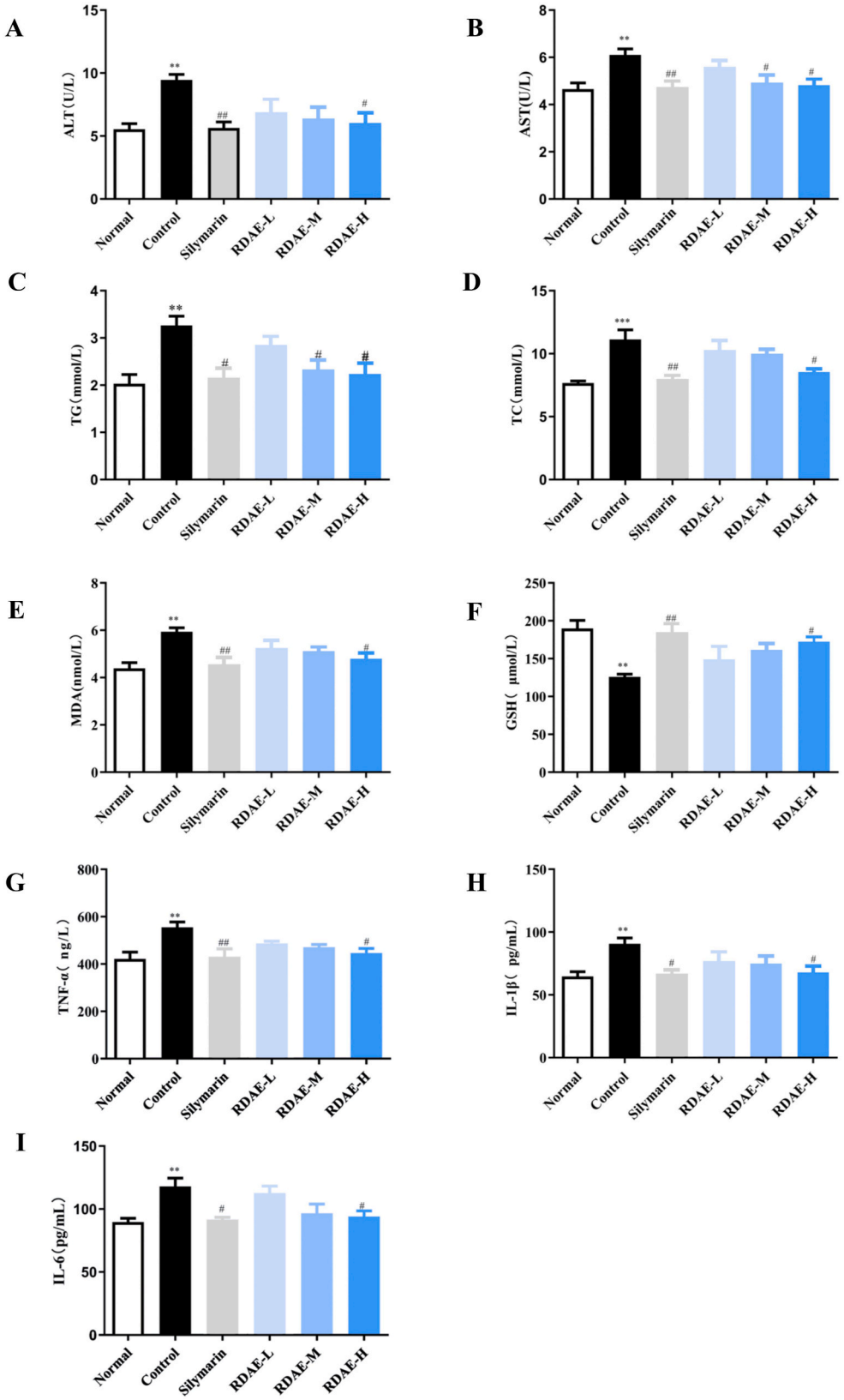

(caption on next page)

Fig. 2. Serum analysis ($\bar{x} \pm s$, **n = 10**). (A) ALT, (B) AST, (C) TG, (D) TC, (E) MDA, (F) GSH, (G) TNF-α, (H) IL-1β, (I) IL-6. Normal: blank, Control: model, Silymarin: positive, RDAE-L: low-dose RADE, RDAE-M: medium-dose RADE, RDAE-H: high-dose RADE. $^{*}P < 0.05$, $^{**}P < 0.01$ *vs.* Normal group. $^{\#}P < 0.05$, $^{\#\#}P < 0.01$ *vs.* Control group.

Prism 8.0.2 (GraphPad Software Inc., San Diego, CA, USA), with $P < 0.05$ set as the threshold for statistical significance.

4. Results

4.1. Quality representation of RDAE

The major monomeric components, including lutidine and kaempferol, of the total flavone of RDAE were determined using HPLC (Fig. 1B) for quality representation of RDAE. The precision, repeatability, stability, and spiked recovery of the method were analyzed, and the method was found to be feasible and met the methodological requirements. The standard curves of lutidine and kaempferol were Y = 334.67X + 27.626 (R = 0.9997) and Y = 1053X + 0.52.021 (R = 0.9995), and their contents were 166.5 ± 2.82 and 0.025 ± 5.82 mg/g, respectively.

4.2. RDAE improves body mass and histopathologic changes in the liver tissue of mice with acute ALD

Compared to the normal group, the control group showed a significant reduction in the body mass of the mice ($P < 0.01$). After administration of medium- and high-dose RDAE, body mass was significantly increased ($P < 0.05$) (Fig. 1C).

In contrast, the liver index was significantly increased after modeling acute ALD ($P < 0.01$), but remarkably decreased following the administration of medium- and high-dose RDAE ($P < 0.05$) (Fig. 1D).

The results of HE staining revealed that mice in the Normal group presented with normal liver cells, which were arranged neatly and tightly without inflammatory infiltration, significant degeneration, or necrosis. In the Control group, there were some vacuolar-type liver cells, and the cell cords were disordered, with inflammatory infiltration. Following RDAE administration, the number of vacuolar-type liver cells reduced, and the liver cells tended to be closely arranged, with decreased inflammatory infiltration (Fig. 1E).

Oil-Red-O staining analysis revealed the absence of lipid accumulation and cell infiltration in the Normal group, while some liver cells exhibited red lipid droplets with severe necrosis. However, treatment with RDAE resulted in a reduction of hepatic lipid droplet accumulation (Fig. 1F).

TUNEL results showed that the apoptosis rate of hepatocytes in RDAE group was significantly reduced compared with Control group (Fig. 1G).

RDAE could improve inflammatory infiltration and lipid accumulation in liver cells in mice with acute ALD by improving body mass and liver index.

4.3. RDAE improves the serum aminotransferases, liver lipid metabolism, and antioxidant levels in mice with acute ALD

The expression levels of serum enzymes associated with liver injury were measured. Serum levels of ALT and AST were significantly higher in the Control group than in the Normal group ($P < 0.01$). In comparison with the Control group, the serum ALT level was remarkably reduced in the RDAE-H group ($P < 0.05$), and the serum AST level was significantly decreased in both the RDAE-M and RDAE-H groups ($P < 0.05$) (Fig. 2A–B).

Hepatic TG and TC levels, which are indicative of lipid metabolism, were examined. The TG ($P < 0.01$) and TC ($P < 0.001$) levels significantly increased after modeling acute ALD. In contrast, remarkable reductions in TG (RDAE-M and RDAE-H, $P < 0.05$) and TC (RDAE-H, $P < 0.05$) contents were noted after RDAE administration (Fig. 2C–D).

In addition, the serum levels of MDA and reduced GSH, products of lipid peroxidation, were tested. Increased serum MDA and decreased GSH levels were observed after acute ALD ($P < 0.01$), whereas reduced MDA and increased GSH levels were observed after administration of high-dose RDAE ($P < 0.05$) (Fig. 2E–F).

4.4. RDAE reduces the levels of serum inflammatory factors in mice with acute ALD

Modeling of acute ALD significantly increased TNF-α, IL-1β, and IL-6 levels ($P < 0.01$ or $P < 0.05$), suggesting that alcohol consumption could induce inflammatory injury in liver cells. Following high-dose RDAE administration, all three indicators were remarkably reduced ($P < 0.05$) (Fig. 2G–I). The results indicated that RDAE could reduce the serum levels of the inflammatory factors TNF-α, IL-1β, and IL-6 in mice with acute ALD.

4.5. RDAE affects the liver metabolic profile in mice with acute ALD

4.5.1. Multivariate statistical analysis

A total of 929 metabolites were identified in PIM and negative ion mode (NIM), including 510 in PIM and 419 in NIM. There were 61 differential metabolites between the Normal and Control groups, 35 between the RDAE-H and Control groups, and 50 between the SIL and Control groups. The metabolites identified in PIM accounted more amongst the total metabolites and therefore were selected

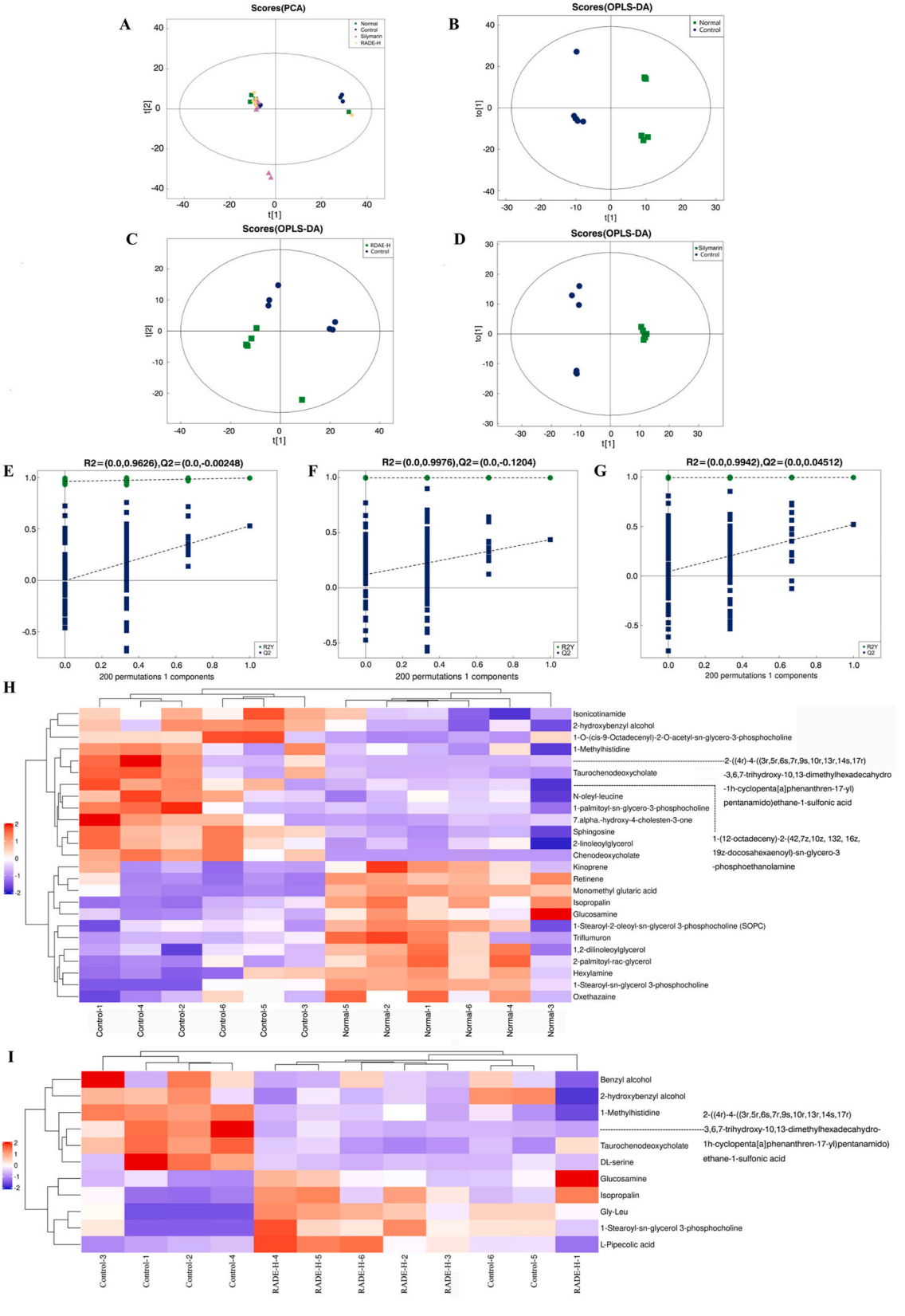

(caption on next page)

Fig. 3. Liver metabolomic analysis. (A) PCA and OPLS-DA plots of mice in each group, (B) OPLS-DA score plots between normal and control in positive ion mode, (C) OPLS-DA score plots between RADE-H and control in positive ion mode, (D) OPLS-DA score plots between Silymarin and control in positive ion mode, (E) 200-Time permutations were performed and plotted between normal and control in positive ion mode, (F) 200-Time permutations were performed and plotted between RADE-H and control in positive ion mode, (G) 200-Time permutations were performed and plotted between Silymarin and control in positive ion mode, (H) Heat map of different metabolites between normal and control, (I) Heat map of different metabolites between RADE-H and control. Normal: blank, control: model, silymarin: positive, RDAE-L: low-dose RADE, RDAE-M: medium-dose RADE, RDAE-H: high-dose RADE.

for further analysis.

Unsupervised principal component analysis (PCA) can reflect the original information, whereas supervised orthogonal partial least-squares discriminant analysis (OPLS-DA) can intuitively reveal the clustering and trajectory of each sample. In metabolomics, PCA plots can reflect the overall degree of variation that considers the metabolic differences between groups. Here, PCA plots of the Blank, Control, SIL, and RDAE-H groups (the RDAE-H group was selected owing to its stronger pharmacological effect) were obtained, which revealed significant separation between the groups (Fig. 3A).

The results of OPLS-DA demonstrated significant separation between the Normal and Control, SIL and Control, and RDAE-H and Control groups, suggesting that the control was stable with high confidence and good predictive performance (Fig. 3B–D). Validation was performed to avoid overfitting. The Q^2 intercept of the model was smaller than 0. The R^2 and Q^2 of the model for the Control and Normal groups were 0.9626 and −0.00248, respectively, while those for the Control and SIL groups were 0.9967 and 0.1204, respectively. In the context of differentiating the Control from the RDAE-H groups, the R^2 and Q^2 were 0.9942 and 0.04512, respectively. R^2 represents the linear fit of the data, and a value closer to 1 indicates better model fit. These results indicate that the model was effective and reliable (Fig. 3E–G).

4.5.2. Screening of differential metabolites

A total of 34 differentially expressed metabolites were identified. Between the Normal and Control groups, there were 25 differential metabolites, including 13 metabolites (chenodeoxycholic acid, tauroursodeoxycholate, leucine oleyl, etc.) with increased content, and 12 metabolites (e.g., 1, 2-dioleacylglycerol, hexylamine) with decreased content in the liver tissue of the Control group. It was suggested that the 25 endogenous differential metabolites might be potential biomarkers for predicting ethanol-induced alcoholic liver injury in mice. After RDAE administration, 11 metabolites were differentially expressed, among which dichloropyridine ester acetate, glucosamine, 1-stearyl-*sn*-glycerol-3-choline phosphate, glycine-$_L$-leucine, and L-2-piperidinic acid were more abundant,

Table 1
Comparison of metabolites between different groups.

	Diffffferential metabolites	Normal *vs.* Control up-down	Control *vs.* RDAE-H up-down
1	Chenodeoxycholate	Up	–
2	2-((4r)-4-((3r,5r,6s,7r,9s,10r, 13r,1 4s,17r) −3,6,7-trihydroxy-10,13-dimethylhexadecahydro-1 h-cyclopenta[*a*]phenanthren-17-yi)pentanamido)ethane-1-sulfonic acid	Up	Down
3	Taurochenodeoxycholate	Up	–
4	1-*O*-(*cis*-9-Octadecenyi)-2-*O*-acetyl-*sn*-glycero-3-phosphocholine	Up	–
5	N-oleyl-leucine	Up	–
6	7.alpha.-hydroxy-4-cholesten-3-one	Up	–
7	1-(1 z-octadeceny)-2-(4z.7z.10z, 13z, 16z, 19z-docosahexaenoyl)-*sn*-glycero-3-phosphoethanolamine	Up	–
8	2-linoleoviglycerol	Up	–
9	Sphingosine	Up	–
10	1-Methylhistidine	Up	–
11	1-palmitoyl-*sn*-glycero-3-phosphocholine	Up	–
12	2-hydroxybenzyl alcoho	Up	Down
13	Isonicotinamide	Up	–
14	1,2-dilinoleoyiglycerol	Down	–
15	Hexylamine	Down	–
16	Oxethazaine	Down	–
17	2-palmitoyl-rac-giycerol	Down	–
18	Monomethyl glutaric acid	Down	–
19	1-Stearoy1-2-oleoyl-*sn*-glycerol 3-phosphocholine (SOPC)	Down	–
20	Glucosamine	Down	Up
21	1-Stearoyl-*sn*-glycerol 3-phosphocholine	Down	Up
22	Isopropaiin	Down	Up
23	Triflumuron	Down	–
24	Retinene	Down	–
28	Gly-Leu	–	Up
29	L-Pipecolic acid	–	Up
30	Benzyl alcohol	–	Down
32	1-Methylhistidine	–	Down
33	Taurochenoceoxycholate	–	Down
34	Ol serine	–	Down

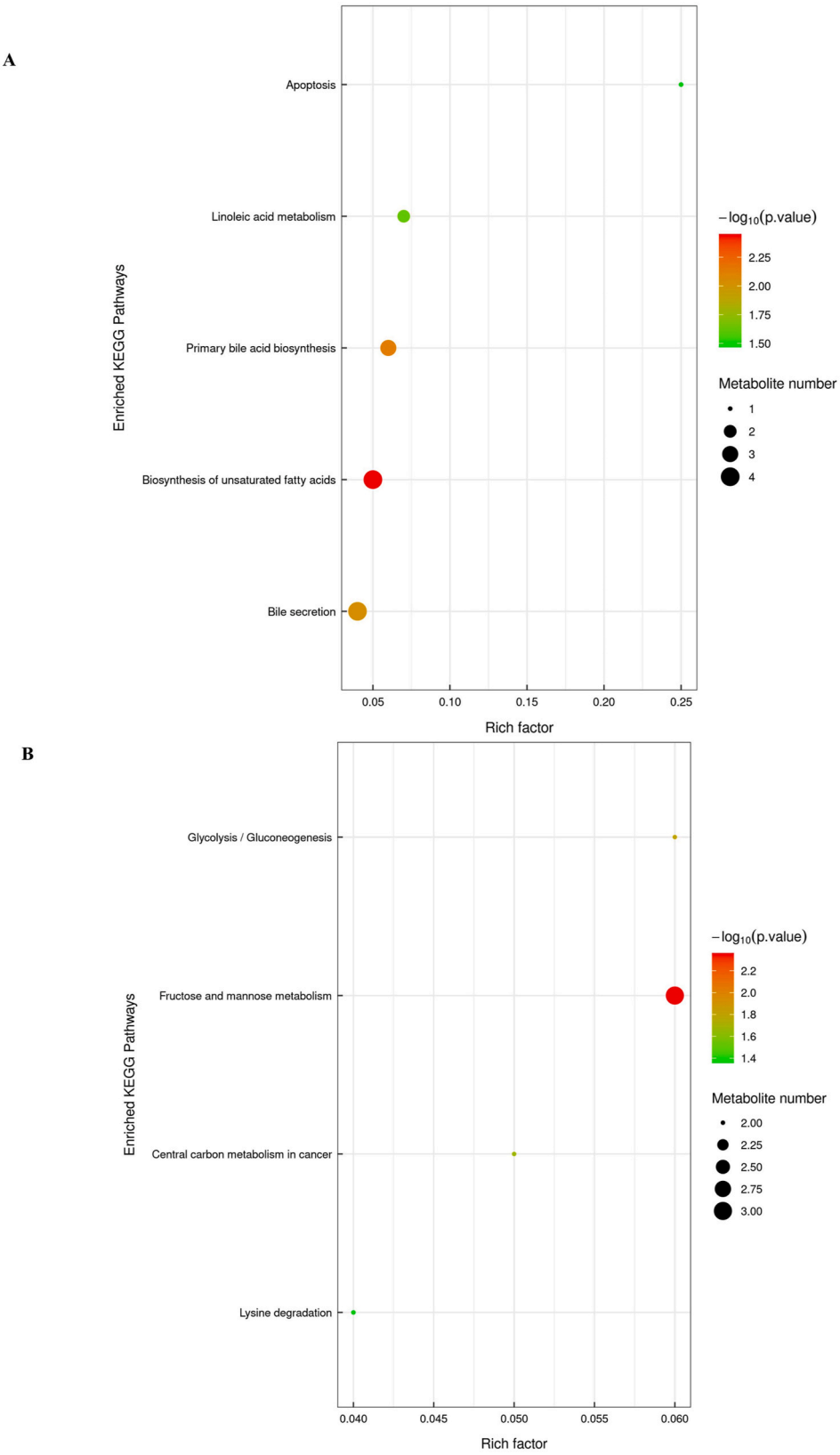

(caption on next page)

Fig. 4. KEGG pathway enrichment analyses. (A) KEGG pathway enrichment analyses of normal and control, (B) KEGG pathway enrichment analyses of RADE-H and control.

whereas benzyl alcohol, salicyl alcohol, 1-methyl-$_{L}$-histidine, taurogoose (deoxygenated) cholate, and $_{DL}$-serine were less abundant (Table 1). Hierarchical clustering was performed to show the differential metabolites more intuitively, and the results are shown as a heatmap (Fig. 3H–I). Collectively, these results demonstrated that high-dose RDAE restored the content of endogenous metabolites at different levels.

4.5.3. Pathway analysis in differential metabolites

Pathway analysis of differential metabolites was conducted using Metabo Analyst 5.0, resulting in nine metabolism-related pathways with differential activity before and after RDAE administration (Fig. 4A–B). These pathways were involved in fructose and mannose metabolism, bile secretion, primary bile acid biosynthesis, linoleic acid metabolism, Glycolysis/Gluconeogenesis, Lysine degradation, and central carbon metabolism in cancer, which revealed the critical significance of amino acid and glucose metabolism in acute ALD.

4.6. RDAE changes the content of amino acids and derivatives in mice with acute ALD

To gain further insight into the role of RDAE in ethanol-induced alcoholic liver injury, 31 specific amino acids were selected and further analyzed. Targeted metabolomic analysis revealed that among the 29 amino acids and derivatives between the Normal and Control groups, leucine, proline, alanine/sarcosine, isoleucine, valine, taurine, choline, tryptophan, glycine, methionine, lysine, serine, hydroxyproline, and ornithine exhibited statistically significant differences ($P < 0.05$). After RDAE administration, a significant increase was observed in the levels of leucine, proline, alanine/sarcosine, isoleucine, valine, taurine, and choline ($P < 0.05$). The changing trend of amino acids is shown in Fig. 5. Additionally, the 29 differential amino acids and derivatives in liver tissue were processed for correlational analysis. The results indicated that leucine had the strongest positive association with other metabolites, whereas creatine, histidine, and arginine had the strongest negative associations with other metabolites (Fig. 6).

4.7. RDAE significantly increases the expression of proteins involved in the MAPKs/NF-κB/COX-2-iNOS signaling pathway in the liver of mice with acute ALD

Following acute ALD modeling, the protein levels of p–NF–κB (p65)/NF-κB (p65), *p*-ERK$_{1/2}$/ERK$_{1/2}$, *p*-JNK/JNK and p-p38/p-38 in the liver tissue were significantly increased ($P < 0.01$, $P < 0.05$). In contrast, the levels of these proteins were reversed by RDAE administration ($P < 0.01$, $P < 0.05$).

In addition, the protein levels of COX-2 and iNOS in the liver tissue exhibited an increasing trend with the occurrence of acute ALD ($P < 0.01$), but they were significantly reduced after administration of medium- and high-dose RDAE ($P < 0.05$, $P < 0.01$) (Fig. 7A–G).

The results suggested that RDAE could inhibit the expression of proteins involved in the MAPKs/NF-κB/COX-2-iNOS signaling pathway at different levels. The effect of high-dose RDAE was better than that of low-dose RDAE, indicating that RDAE is dose-dependent in the treatment of acute ALD.

5. Discussion

Chinese herbal medicines have been used extensively utilized the treatment of acute/chronic metabolic disorders, such as liver injury, due to their multifaceted pharmacological properties, potent therapeutic effects, and minimal adverse reactions. They also constitute a focal point for research on traditional Chinese medicines and functional foods. In this context, our study selected RDAE with anti-inflammatory and hepatoprotective functions for analysis to address the existing gap in an in-depth mechanistic investigation into the therapeutic efficacy of RDAE in liver injury.

During acute alcoholic liver injury, alcohol induces excessive production of reactive oxygen species (ROS), leading to elevated levels of liver lipids [22,23], oxidative stress [24], and release of inflammatory cytokines including TNF-α, IL-6, and IL-1β [25], thereby exacerbating inflammation [26]. In this study, we observed that RDAE mitigated alcohol-induced weight loss and attenuated the increase in liver index. Efficacy analysis revealed that RDAE significantly reduced serum levels of TG, TC, ALT, AST, MDA, and inflammatory factors (TNF-α, IL-1β,and IL-6), while increasing GSH levels in mice with acute ALD. These findings suggest that RDAE can ameliorate alcohol-induced lipid accumulation and oxidative stress while alleviating inflammatory insults in hepatic cells. The effects observed were consistent with those exerted by the SIL-positive agent.

Metabolomics enables a comprehensive analysis of systemic metabolism, while Chinese herbal medicines exhibit holistic therapeutic effects against ALD at various developmental stages. In this study, we employed metabolomic approaches to identify potential early biomarkers for predicting liver injury and metabolic abnormalities by analyzing differential metabolites following liver injury [27]. Currently, mice with ALD are commonly utilized to investigate the metabolic profiles in serum, urine, and liver tissue using techniques such as magnetic resonance (NMR) spectroscopy, gas chromatography-mass spectrometry (GC-MS), and liquid chromatography/tandem mass spectrometry (LC-MS) [28]. Previous studies on ALD analysis using metabolomics have primarily focused on phospholipid metabolism [29], amino acid metabolism [30,31], and energy metabolism [32]. In our present study, non-targeted metabolomics was employed to screen differential metabolites and associated metabolic pathways in mice with acute ALD. We

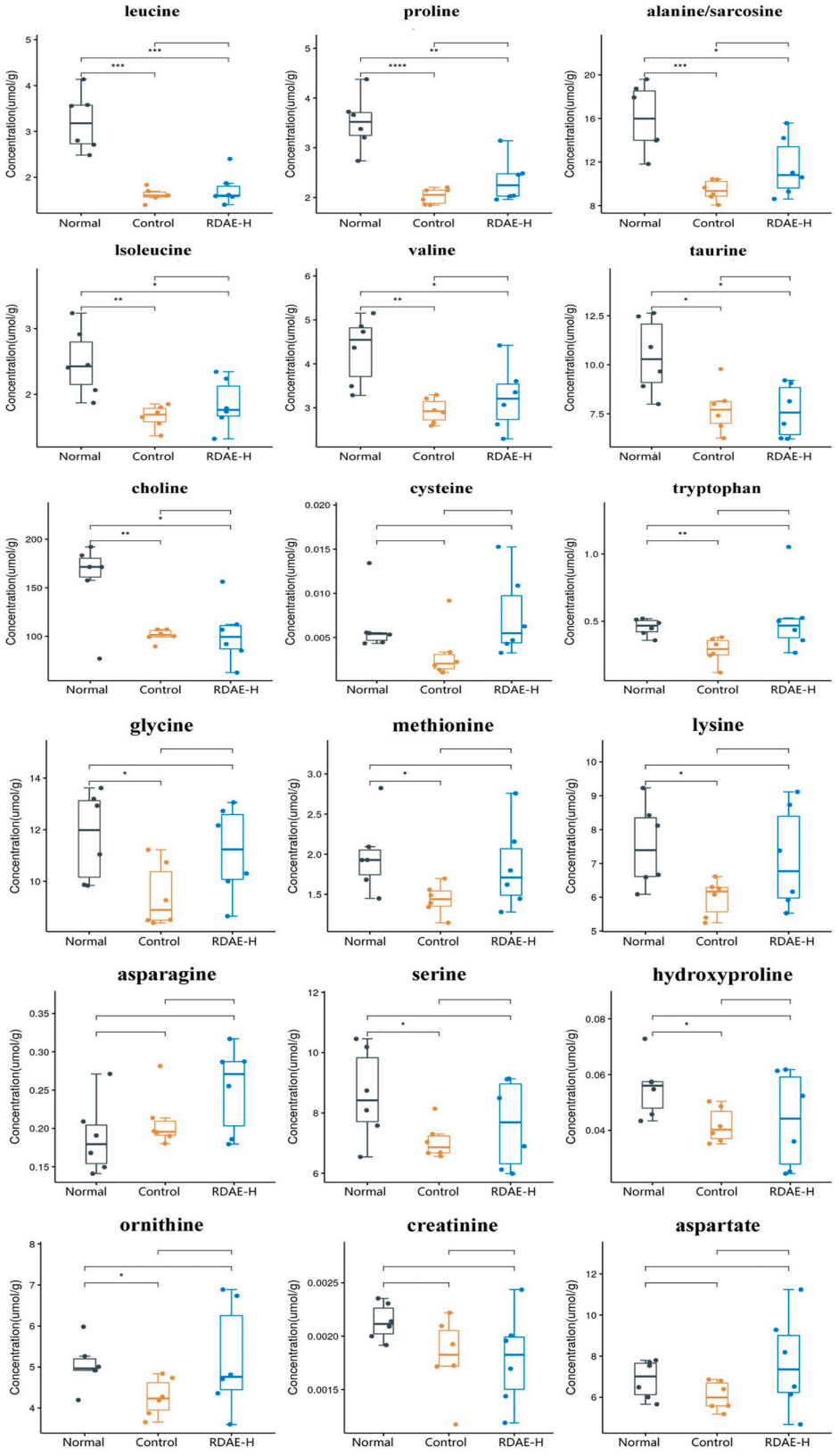

(caption on next page)

Fig. 5. Quantitative analysis of amino acids and their derivatives in liver samples. Normal: blank, Control: model, RDAE-H: high-dose RADE. $^{*}P < 0.05$, $^{**}P < 0.01$, $^{***}P < 0.001$ *vs.* Normal group. $^{\#}P < 0.05$, $^{\#\#}P < 0.01$, $^{\#\#\#}P < 0.001$ *vs.* Control group.

identified 34 differential metabolites and nine related pathways mainly involved in glucose and amino acid metabolism. Following administration of RDAE treatment, the levels of these differential metabolites were restored to varying degrees, facilitating the normalization of the metabolic phenotype within normal ranges. This finding demonstrates that RDAE significantly impacts the metabolism in mice with ALD. Notably, indicators reflecting drug effects such as TG, TC ALT AST GSH MDA exhibited changes after RDAE administration. These results align with those observed for positive SIL agents. Our approach analyzes global indicators which compensate for limitations observed when analyzing typical indicators.

In cases of acute alcoholic liver injury, ethanol causes metabolic abnormalities in glucose, lipids, and amino acids, resulting in a disrupted tricarboxylic acid (TCA) cycle. To investigate this further, we conducted targeted metabolomics analysis on 31 amino acids and their derivatives in liver tissue. Acute alcohol consumption led to decreased levels of isoleucine, leucine, valine and taurine; however, RDAE treatment effectively restored the levels of isoleucine, leucine and valine. Isoleucine, leucine and valine are essential substrates for protein synthesis as branched-chain amino acids (BCAAs), whose oxidation promotes the TCA cycle leading to mitochondrial dysfunction that induces ROS overproduction and activation of the NF-κB pathway promoting inflammatory response and

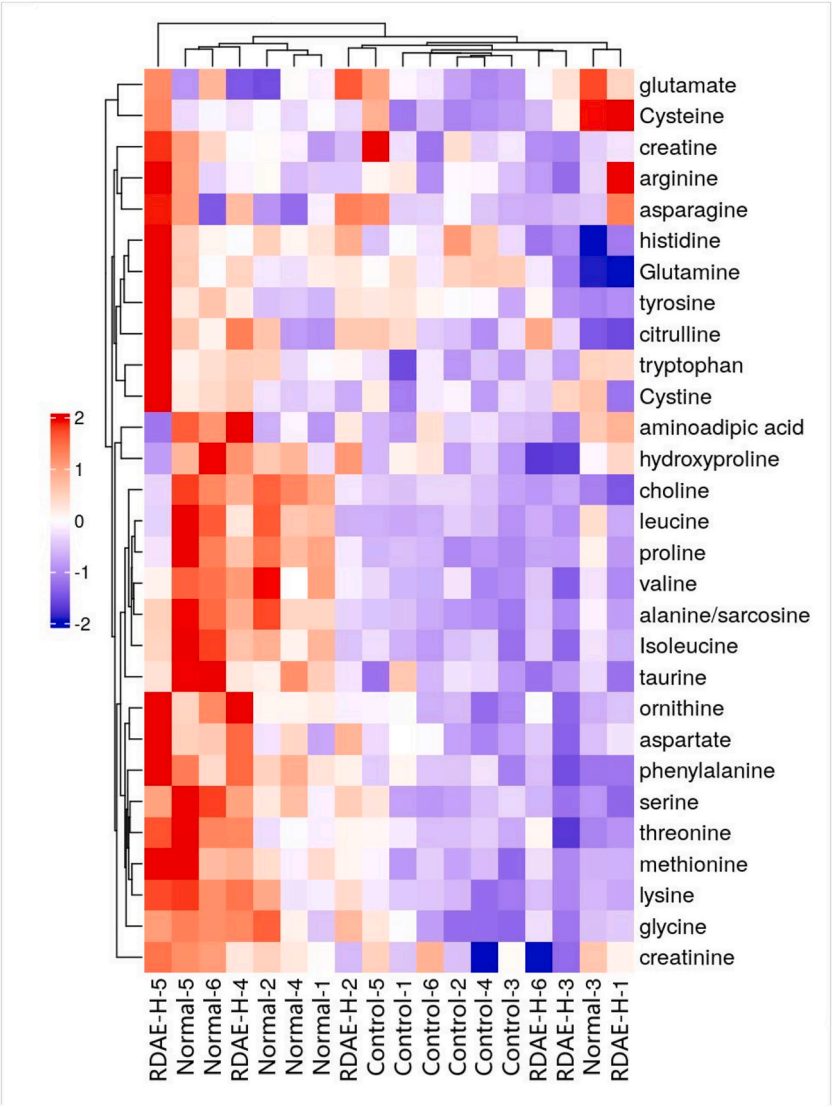

Fig. 6. Differential metabolite heat maps in liver samples. The X- and Y-axes represent variations in amino acids and derivatives, respectively, and a deeper color indicates a stronger correlation. Normal: blank, Control: model, RDAE-H: high-dose RADE. $^{*}P < 0.05$, $^{**}P < 0.01$, $^{***}P < 0.001$ *vs.* Normal group. $^{\#}P < 0.05$, $^{\#\#}P < 0.01$, $^{\#\#\#}P < 0.001$ *vs.* Control group. (For interpretation of the references to color in this figure legend, the reader is referred to the Web version of this article.)

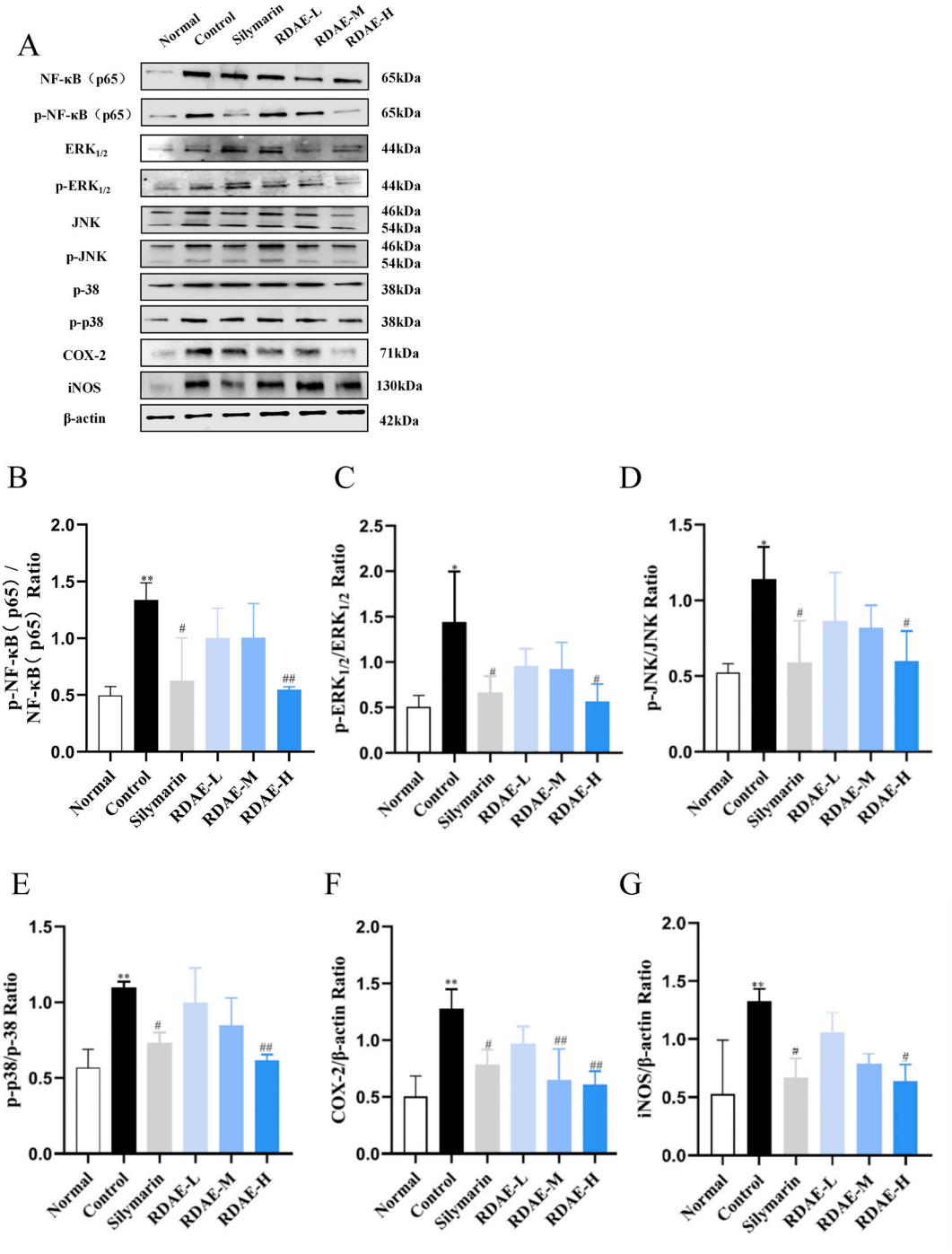

Fig. 7. Aqueous extract from *Rhamnus utilis* Decne inhibited MAPKs/NF-κB/COX-2-iNOS signaling pathway in the liver of mice with acute alcoholic liver injury. The expression was detected by western blotting, and their expression was normalized relative to β-actin ($\bar{x} \pm s$, n = 3). (A) Protein expression of NF-κB(p65), p–NF–κB(p65), $ERK_{1/2}$, *p*-$ERK_{1/2}$, JNK, *p*-JNK, p-p38, p38, COX-2 and iNOS, (B) p–NF–κB(p65)/NF-κB(p65), (C) *p*-$ERK_{1/2}$/$ERK_{1/2}$, (D) *p*-JNK/JNK, (E) p-p38/p38, (F) COX-2/β-actin, (G) iNOS/β-actin. Normal: blank, control: model, silymarin: positive, RDAE-L: low-dose RADE, RDAE-M: medium-dose RADE, RDAE-H: high-dose RADE. $^{*}P < 0.05$, $^{**}P < 0.01$ *vs.* Normal group. $^{\#}P < 0.05$, $^{\#\#}P < 0.01$ *vs.* Control group.

oxidative stress injury in peripheral monocytes and endothelial cells [33,34]. These studies suggest that BCAA levels may reflect inflammatory processes under different pathophysiological states. Compelling evidence shows that patients with alcoholic liver injury have significantly lower levels of isoleucine and leucine compared to healthy individuals [35]. Furthermore, taurine deficiency can

lead to abnormal liver function [36], which might be due to increased taurinolysis caused by elevated oxidative stress improving impaired liver function [37]. Our study yielded consistent results.

Previous studies have reported that during liver injury, stress stimuli, pathogens, or pro-inflammatory factors can induce phosphorylation of essential proteins in the NF-κB (p65) and MAPKs pathways, leading to increased levels of these proteins and subsequent severe oxidative and inflammatory damage [7,38]. The NF-κB signaling pathway plays a crucial role in inflammation regulation [39]. Following inflammation, activated NF-κB translocates to the nucleus where it regulates the iNOS and COX-2 pathways, thereby accelerating inflammatory injury [40,41]. Therefore, the expression of proteins involved in the MAPKs/NF-κB/COX-2-iNOS signaling pathway was also examined using western blotting in this study. Consistently with these findings, our study observed a significant reduction in the expression of p-P38/P-38 and p–NF–κB (p65)/NF-κB (p65) proteins in mouse liver tissue treated with RDAE ($P < 0.05$, $P < 0.001$). These results suggest that RDAE exhibits dose-dependent inhibition on protein expression involved in the MAPKs/NF-κB/COX-2-iNOS signaling pathway, thus alleviating inflammation in acute ALD.

Currently, there is a paucity of literature regarding the pharmacological effects and mechanisms of RDAE. Within Chinese literature, only a limited number of scholars have conducted preliminary investigations in this area. In this study, rutin and naringenin were selected as flavonoid constituents for quality control assessment of RDAE using HPLC analysis. Furthermore, the efficacy indicators for anti-inflammatory activity and hepatoprotection were evaluated. A novel non-targeted metabolomics investigation was performed to analyze the global hepatic metabolic profile in mice with acute alcoholic liver injury, accompanied by targeted analysis of amino acids. The significance of these findings lies in elucidating the potential mechanism underlying RDAE's protective effect against acute alcoholic liver injury, which may involve enhancing lipid metabolism, augmenting antioxidant enzyme activity, suppressing pro-inflammatory cytokine expression and MAPKs/NF-κB/COX-2-iNOS signaling pathways, as well as modulating overall hepatic metabolic profile. Indeed, non-targeted metabolomics results have identified nine major metabolic pathways associated with lipid and glucose metabolism that are crucial for maintaining stable blood glucose levels in the liver and performing digestion, absorption, decomposition, synthesis, and transportation of lipids. However, due to time constraints, limited sample size, and space availability, this study did not extensively explore these findings. In this study, only non-targeted metabolomics techniques and amino acid metabolomics analysis were used to explore the potential pathway of RDAE in the treatment of ALD, providing a possibility to clarify the mechanism of RDAE in the treatment of acute ALD. In addition, there are few studies on RDAE and insufficient observations on monomer compounds, effects on non-targeted metabolomics, and other aspects related to protein pathways, which will be further investigated in future experiments.

6. Conclusion

RDAE has the potential to enhance hepatic function and exert a hepatoprotective effect against acute alcoholic liver injury, potentially through modulation of lipid metabolism, augmentation of antioxidant enzyme activity, suppression of proinflammatory cytokine expression and proteins involved in the MAPKs/NF-κB/COX-2-iNOS signaling pathway, as well as influencing global hepatic metabolic profiling.

Funding

This work was funded by the project of Shanxi Key Laboratory of Traditional Herbal Medicines Processing (no. 202104010910029), the Innovation Team of Shanxi University of Chinese Medicine (no. 2022TD1014), the Discipline Construction of Shanxi University of Chinese Medicine (no. 2018-01) and the Chinese Medicine Science and Technology Innovation Project (NO.CZ2023041-019).

Data availability

The data used to support the results of this study are available from the corresponding author upon request.

CRediT authorship contribution statement

Xianglong Meng: Writing – review & editing, Writing – original draft, Methodology, Data curation, Conceptualization. **Kele Ren:** Writing – review & editing, Writing – original draft, Methodology, Data curation, Conceptualization. **Xiaoqin Liu:** Resources, Investigation, Conceptualization. **Chenzi Lyu:** Resources. **Hyo Won Jung:** Supervision. **Yilong Zhang:** Project administration. **Shuosheng Zhang:** Supervision, Project administration.

Declaration of competing interest

The authors declare that they have no known competing financial interests or personal relationships that could have appeared to influence the work reported in this paper.

Acknowledgements

We express our gratitude to all of the participants in the study.

Appendix A. Supplementary data

Supplementary data to this article can be found online at https://doi.org/10.1016/j.heliyon.2024.e32523.

References

[1] X. Wang, K. Dong, Y. Ma, Q. Jin, S. Yin, S. Wang, Hepatoprotective effects of chamazulene against alcohol-induced liver damage by alleviation of oxidative stress in rat models, Open Life Sci. 15 (1) (2020), https://doi.org/10.1515/biol-2020-0026.

[2] T.N. Bukong, A. Iracheta-Vellve, B. Gyongyosi, A. Ambade, D. Catalano, K. Kodys, G. Szabo, Therapeutic benefits of spleen tyrosine kinase inhibitor administration on binge drinking-induced alcoholic liver injury, steatosis, and inflammation in mice, Alcohol Clin. Exp. Res. 40 (7) (2016), https://doi.org/10.1111/acer.13096.

[3] A. Peacock, J. Leung, S. Larney, S. Colledge, M. Hickman, J. Rehm, G.A. Giovino, R. West, W. Hall, P. Griffiths, R. Ali, L. Gowing, J. Marsden, A.J. Ferrari, J. Grebely, M. Farrell, L. Degenhardt, Addiction, Global Statistics on Alcohol, Tobacco and Illicit Drug Use: 2017 Status Report, vol. 113, 2018, https://doi.org/10.1111/add.14234. Issue 10.

[4] J.M. Ludwig, Y. Zhang, W. Chamulitrat, W. Stremmel, A. Pathil, Anti-inflammatory properties of ursodeoxycholyl lysophosphatidylethanolamide in endotoxin-mediated inflammatory liver injury, PLoS One 13 (5) (2018), https://doi.org/10.1371/journal.pone.0197836.

[5] R. Yuan, X. Tao, S. Liang, Y. Pan, L. He, J. Sun, J. Wenbo, X. Li, J. Chen, C. Wang, Protective effect of acidic polysaccharide from Schisandra chinensis on acute ethanol-induced liver injury through reducing CYP2E1-dependent oxidative stress, Biomed. Pharmacother. 99 (2018), https://doi.org/10.1016/j.biopha.2018.01.079.

[6] Q. Zhu, H. Zhuo, L. Yang, H. Ouyang, J. Chen, B. Liu, H. Huang, A peptide HEPFYGNEGALR from apostichopus japonicus alleviates acute alcoholic liver injury by enhancing antioxidant response in male C57BL/6J mice, Molecules 27 (18) (2022), https://doi.org/10.3390/molecules27185839.

[7] L. Xu, Y. Yu, R. Sang, J. Li, B. Ge, X. Zhang, Protective effects of taraxasterol against ethanol-induced liver injury by regulating CYP2E1/Nrf2/HO-1 and NF-κB signaling pathways in mice, Oxid. Med. Cell. Longev. (2018), https://doi.org/10.1155/2018/8284107, 2018.

[8] A. Namachivayam, A. Valsala Gopalakrishnan, A review on molecular mechanism of alcoholic liver disease, Life Sci. 274 (2021), https://doi.org/10.1016/j.lfs.2021.119328.

[9] R. Huang, Y. Sun, R. Liu, B. Zhu, H. Zhang, H. Wu, ZeXieYin formula alleviates atherosclerosis by inhibiting the MAPK/NF-κB signaling pathway in APOE-/- mice to attenuate vascular inflammation and increase plaque stability, J. Ethnopharmacol. 327 (2024 Mar 2) 117969, https://doi.org/10.1016/j.jep.2024.117969. Epub ahead of print. PMID: 38437888.

[10] X. Zhang, Z. Dong, H. Fan, Q. Yang, G. Yu, E. Pan, N. He, X. Li, P. Zhao, M. Fu, J. Dong, Scutellarin prevents acute alcohol-induced liver injury via inhibiting oxidative stress by regulating the Nrf2/HO-1 pathway and inhibiting inflammation by regulating the AKT, p38 MAPK/NF-κB pathways, J. Zhejiang Univ. - Sci. B 24 (7) (2023 Mar 25) 617–631, https://doi.org/10.1631/jzus.B2200612. PMID: 37455138; PMCID: PMC10350365.

[11] committee. CMMe, Chinese Materia Medica, Shanghai Science and Technology Publishing House, 1999.

[12] X. Gao, The Antioxidant Activity, Antimicrobial Activity and Extraction of Flavonoids of Leaves of Rhamnus Utilis, Shanxi University, 2015.

[13] D. Sun, Composition and Antioxidative and Bacteriostatic Activities of Flavonoids from Rhamnus Utilis Leaves, Shanxi University, 2020.

[14] Q. Ma, Extraction and Purification of Polyphenols from Rhamnus Utilis Leaves and Analysis of Antioxidant Activity, Shanxi University, 2021.

[15] L. Zhang, Purification of Flavonoids from Rhamnus Utilis Fruits and its Protective Effect on Acute Liver Injury Induced by CCk in Mice, Shanxi University, 2019.

[16] Z. Shi, Protective Effects of Flavonoids from Fruits of Rhamnus Utilis on Alcoholic Liver Injury in Mice and Antioxidant Activities, Shanxi University, 2018.

[17] X. Wang, J. Li, X. Yang, X.M. Gao, H. Wang, Y.X. Chang, A rapid and efficient extraction method based on industrial MCM-41-miniaturized matrix solid-phase dispersion extraction with response surface methodology for simultaneous quantification of six flavonoids in Pollen typhae by ultra-high-performance liquid chromatography, J. Separ. Sci. 42 (14) (2019) 2426–2434, https://doi.org/10.1002/jssc.201900227.

[18] M. Miao, L. Kang, X. Fang, Standard (draft) for preparation of alcoholic liver injury animal model, China Journal of Traditional Chinese Medicine and Pharmacy 33 (3) (2018) 1000–1003. https://kns.cnki.net/kcms2/article/abstract?v=TzO8JwpG6ui7o5aLZ4mjfHB9V2irPq64nPSNHbusMQq2iPlCa8EioObtuds0HUj1nhaTuu3fFFwdc3oX69f8wBdjly1mAyaU9gq8YJ8lRCdVWSTQGEKXjbhoyGfa3HnwfPpvjNWJG4VfJZEmLzxKXg==&uniplatform=NZKPT&language=CHS.

[19] A. Lamas-Paz, M. Mesquita, M. Garcia-Lacarte, et al., Fecal microbiota transplantation from female donors restores gut permeability and reduces liver injury and inflammation in middle-aged male mice exposed to alcohol, Front. Nutr. 11 (2024) 1393014, https://doi.org/10.3389/fnut.2024.1393014. Published 2024 Apr 18.

[20] X. Liu, X. Meng, X. Su, K. Ren, C. Ning, X. Qi, S. Zhang, The mechanism of ginger and its processed products in the treatment of estradiol valerate coupled with oxytocin-induced dysmenorrhea in mice via regulating the TRP ion channel-mediated ERK(1/2)/NF-κB signaling pathway, Food Funct. 13 (21) (2022) 11236–11248. http://doi:10.1039/d2fo01845d.

[21] X. Meng, J. Yan, J. Ma, A.N. Kang, S.Y. Kang, Q. Zhang, C. Lyu, Y.K. Park, H.W. Jung, S. Zhang, Effects of Jowiseungki-tang on high fat diet-induced obesity in mice and functional analysis on network pharmacology and metabolomics analysis, J. Ethnopharmacol. 283 (2022), https://doi.org/10.1016/j.jep.2021.114700.

[22] P. Fehér, Z. Ujhelyi, M. Vecsernyés, F. Fenyvesi, G. Damache, A. Ardelean, M. Costache, A. Dinischiotu, A. Hermenean, I. Bacskay, Hepatoprotective effects of a self-micro emulsifying drug delivery system containing Silybum marianum native seed oil against experimentally induced liver injury, Pharmazie 70 (4) (2015), https://doi.org/10.1691/ph.2015.4146.

[23] J.Y. Qiao, H.W. Li, F.G. Liu, Y.C. Li, S. Tian, L.H. Cao, K. Hu, X.X. Wu, M.S. Miao, Effects of portulaca oleracea extract on acute alcoholic liver injury of rats, Molecules 24 (16) (2019), https://doi.org/10.3390/molecules24162887.

[24] S. Li, H.Y. Tan, N. Wang, Z.J. Zhang, L. Lao, C.W. Wong, Y. Feng, The role of oxidative stress and antioxidants in liver diseases, Int. J. Mol. Sci. 16 (11) (2015), https://doi.org/10.3390/ijms161125942.

[25] Y. Xue, X. Li, Y. Tian, X. Huang, L. Zhang, J. Li, H. Hou, P. Dong, J. Wang, Salmon sperm DNA prevents acute liver injury by regulating alcohol-induced steatosis and restores chronic hepatosis via alleviating inflammation and apoptosis, J. Food Biochem. 46 (10) (2022), https://doi.org/10.1111/jfbc.14346.

[26] M. Nakayama, M. Naito, K. Omori, S. Ono, K. Nakayama, N. Ohara, Porphyromonas gingivalis gingipains induce cyclooxygenase-2 expression and prostaglandin E(2) production via ERK1/2-activated AP-1 (c-Jun/c-Fos) and IKK/NF-κB p65 cascades, J. Immunol. 208 (5) (2022) 1146–1154. https://doi:10.4049/jimmunol.2100866.

[27] M. Kyriakides, L. Maitre, B.D. Stamper, I. Mohar, T.J. Kavanagh, J. Foster, I.D. Wilson, E. Holmes, S.D. Nelson, M. Coen, Comparative metabonomic analysis of hepatotoxicity induced by acetaminophen and its less toxic meta-isomer, Arch. Toxicol. 90 (12) (2016), https://doi.org/10.1007/s00204-015-1655-x.

[28] X. Fan, X. Wang, J. Lian, Z. Pei, M. Jiang, M. Bai, Flos carthami exerts hepatoprotective action in a rat model of alcoholic liver injury via modulating the metabolomics profile, Evid. base Compl. Alternative Med. (2022), https://doi.org/10.1155/2022/8158699, 2022.

[29] W. Zhang, W. Zhong, Q. Sun, X. Sun, Z. Zhou, Adipose-specific lipin1 overexpression in mice protects against alcohol-induced liver injury, Sci. Rep. 8 (1) (2018), https://doi.org/10.1038/s41598-017-18837-2.

[30] H.L. Zeng, Q. Yang, H. Du, H. Li, Y. Shen, T. Liu, X. Chen, G.M. Kamal, Q. Guan, L. Cheng, J. Wang, F. Xu, Proteomics and metabolomics analysis of hepatic mitochondrial metabolism in alcohol-preferring and non-preferring rats, Oncotarget 8 (60) (2017), https://doi.org/10.18632/oncotarget.22040.

[31] T. Ma, Y. Li, Y. Zhu, S. Jiang, C. Cheng, Z. Peng, L. Xu, Differential metabolic pathways and metabolites in a C57BL/6J mouse model of alcoholic liver disease, Med. Sci. Mon. Int. Med. J. Exp. Clin. Res. 26 (2020), https://doi.org/10.12659/MSM.924602.

[32] H. Fang, A. hua Zhang, H. Sun, J. bo Yu, L. Wang, X. jun Wang, High-throughput metabolomics screen coupled with multivariate statistical analysis identifies therapeutic targets in alcoholic liver disease rats using liquid chromatography-mass spectrometry, J. Chromatogr., B: Anal. Technol. Biomed. Life Sci. 1109 (2019), https://doi.org/10.1016/j.jchromb.2019.01.017.

[33] O. Zhenyukh, E. Civantos, M. Ruiz-Ortega, M.S. Sánchez, C. Vázquez, C. Peiró, J. Egido, S. Mas, High concentration of branched-chain amino acids promotes oxidative stress, inflammation and migration of human peripheral blood mononuclear cells via mTORC1 activation, Free Radic. Biol. Med. 104 (2017), https://doi.org/10.1016/j.freeradbiomed.2017.01.009.

[34] O. Zhenyukh, M. González-Amor, R.R. Rodrigues-Diez, V. Esteban, M. Ruiz-Ortega, M. Salaices, S. Mas, A.M. Briones, J. Egido, Branched-chain amino acids promote endothelial dysfunction through increased reactive oxygen species generation and inflammation, J. Cell Mol. Med. 22 (10) (2018), https://doi.org/10.1111/jcmm.13759.

[35] S. Mukherjee, K. Vaidyanathan, D.M. Vasudevan, S.K. Das, Role of plasma amino acids and GABA in alcoholic and non-alcoholic fatty liver disease - a pilot study, Indian J. Clin. Biochem. 25 (1) (2010), https://doi.org/10.1007/s12291-010-0007-0.

[36] C. Wen, F. Li, L. Zhang, Y. Duan, Q. Guo, W. Wang, S. He, J. Li, Y. Yin, Taurine is involved in energy metabolism in muscles, adipose tissue, and the liver, Mol. Nutr. Food Res. 63 (Issue 2) (2019), https://doi.org/10.1002/mnfr.201800536.

[37] U. Seidel, P. Huebbe, G. Rimbach, Taurine: a regulator of cellular redox homeostasis and skeletal muscle function, Mol. Nutr. Food Res. 63 (Issue 16) (2019), https://doi.org/10.1002/mnfr.201800569.

[38] W. Zhang, J. Yang, J. Liu, X. Long, X. Zhang, J. Li, C. Hou, Red yeast rice prevents chronic alcohol-induced liver disease by attenuating oxidative stress and inflammatory response in mice, J. Food Biochem. 45 (4) (2021), https://doi.org/10.1111/jfbc.13672.

[39] M. Zhao, J. Chen, P. Zhu, M. Fujino, T. Takahara, S. Toyama, A. Tomita, L. Zhao, Z. Yang, M. Hei, L. Zhong, J. Zhuang, S. Kimura, X.K. Li, Dihydroquercetin (DHQ) ameliorated concanavalin A-induced mouse experimental fulminant hepatitis and enhanced HO-1 expression through MAPK/Nrf2 antioxidant pathway in RAW cells, Int. Immunopharm. 28 (2) (2015), https://doi.org/10.1016/j.intimp.2015.04.032.

[40] H. Yu, L. Lin, Z. Zhang, H. Zhang, H. Hu, Targeting NF-κB pathway for the therapy of diseases: mechanism and clinical study, Signal Transduct. Targeted Ther. 5 (Issue 1) (2020), https://doi.org/10.1038/s41392-020-00312-6.

[41] C.J. Liou, W. bin Len, S.J. Wu, C.F. Lin, X.L. Wu, W.C. Huang, Casticin inhibits COX-2 and iNOS expression via suppression of NF-κB and MAPK signaling in lipopolysaccharide-stimulated mouse macrophages. *Journal of Ethnopharmacology*, PART A (2014), https://doi.org/10.1016/j.jep.2014.10.046.